ELECTRONIC SUPPLEMENTARY INFORMATION for

The Interplay Among Gas, Liquid and Solid Interactions Determines the Stability of Surface Nanobubbles

Marco Tortora,[†] Simone Meloni,[*,†,§] Beng Hau Tan,[‡,‖] Alberto Giacomello,[†] Claus-Dieter Ohl,[¶] and Carlo Massimo Casciola[†]

[†]*Dipartimento di Ingegneria Meccanica e Aerospaziale, Università di Roma* La Sapienza, *Via Eudossiana 18, 00184 Roma, Italy*

[‡]*Low Energy Electronic Systems, Singapore-MIT Alliance for Research and Technology, 1 Create Way, 138602 Singapore*

[¶]*Department for Soft Matter, Institute of Physics, Otto-von-Guericke University Magdeburg, 39106 Magdeburg, Germany*

[§]*Dipartimento di Scienze Chimiche e Farmaceutiche (DipSCF), Università degli Studi di Ferrara (Unife), Via Luigi Borsari 46, I-44121, Ferrara, Italy*

[‖]*School of Mechanical and Aerospace Engineering, Nanyang Technological University, 50 Nanyang Avenue, 639798 Singapore*

E-mail: simone.meloni@unife.it

1   Estimation of the Free-Energy Error

The error on a derived observable $O = O(s)$, with s the variable that is directly measured, is usually obtained by error propagation:

$$\delta O^2 = \left(\frac{dO}{ds}\delta s\right)^2 \tag{1}$$

where δs^2 and δO^2 are the variances of s and the estimated variance of O, respectively. δO obtained by error propagation is an upper bound of the actual error of the derived observable. In free energy calculations *via* RMD or similar techniques, in which the free energy $G(z)$ is obtained by numerical integration of the mean force dG/dN, Eq. [**??**], error propagation brings to a severe overestimation of the error on $G(z)$:

$$\delta G(z_j)^2 = \sum_{i=1,j} \frac{\delta G'(z_i)^2 + \delta G'(z_{i-1})^2}{2}(z_i - z_{i-1})^2 \tag{2}$$

Here, like in previous works,[1–6] we use a different approach. We divide the configurations used to estimate $dG(z)/dz$ in M smaller sets from which we obtain the corresponding estimates of the mean force $\{dG_i(z)/dz\}_{i=1,M}$. Frome these, by numerical integration, one obtains a set of free energy curves $\{G_i(z)\}_{1=1,M}$ that can be used to directly compute the variance $\delta G_i(z)^2$ at each value of z :

$$\delta G_i(z)^2 = 1/(M-1) \sum_{i=1,M} (G_i(z) - G(z))^2, \tag{3}$$

where $G(z) = 1/M \sum_{i=1,M} G_i(z)$ is the free energy computed with the complete set of atomistic configurations. Then, one can obtain the error on $G(z)$, taking properly into account correlation effects, using either the *block average* or the *Jackknife* method.[7]

2 The Tan-An-Ohl local oversaturation theory of nanobubbles' stability

The Tan-An-Ohl local oversaturation theory of nanobubbles' stability[8] is an extension of the Lohse and Zhang pinning-oversaturation theory[9]. Eq.[1], the key result of the Tan-An-Ohl theory, is obtained starting from the evolution equation for a dissolving pinned surface nanobubble in a liquid. This problem is analogous to that of an evaporating droplet of liquid, whose exact solution given by Popov[10] has been adapted by Lohse and Zhang[9] to the case of a dissolving spherical cap pinned nanobuble. Lohse and Zhang have obtained the rate of mass change in the hypothesis that the oversaturation ζ is constant through the liquid. By setting the rate of mass change to zero, one obtains the stationarity condition. Tan, An e Ohl.[8] have waived the condition that ζ is constant through the liquid, and Eq. [??] represents the stationarity condition for a surface nanobubble if the oversaturation depends on the distance from the solid substrate, $\zeta(z)$.

3 Relation between force field parameters and gas solubility

Following ref. [11], dissolving a gas in a liquid consisting of two steps: i) creation of a liquid cavity that accommodates a gas molecule and ii) introduction of a gas molecule into the cavity. After its introduction into the cavity, the gas molecule interacts with the surrounding solvent. For very dilute solutions, like air dissolved in water, one can show that: $RT \log K_H = G_c + G_i + RT \log(RT/V_s^0)$; K_H is the Henry's law constant, which relates the amount of gas dissolved in the solvent and its partial pressure: to a higher value of K_H corresponds a higher gas solubility; G_c and G_i are the molar free energies for forming a cavity of prescribed size and inserting a molecule in the cavity, corresponding to steps 'i' and 'ii' of the process outlined above; finally, V_s^0 is the molar volume of the solvent and R is the gas constant. Following Reiss et al [12], G_c depends on the characteristic size σ_s of the solvent and solute molecules, which does not change, while G_i depends on the characteristic energy, ϵ, which we increase of a factor 3. Considering that $G_i = -3.555\pi \, \rho \, R \, \sigma^3 \, \epsilon \, /k_B$ [11], where ρ is the solvent number density and k_B is the Boltzmann constant, the ratio between the Henry's law constants of two solutions differing in the characteristic interaction energy between the solvent and solute by $\Delta\epsilon = \epsilon' - \epsilon''$ is $K_H'/K_H'' = \exp[-3.555\pi \, \rho \, R \, \sigma^3 \, \Delta\epsilon \, /k_B]$
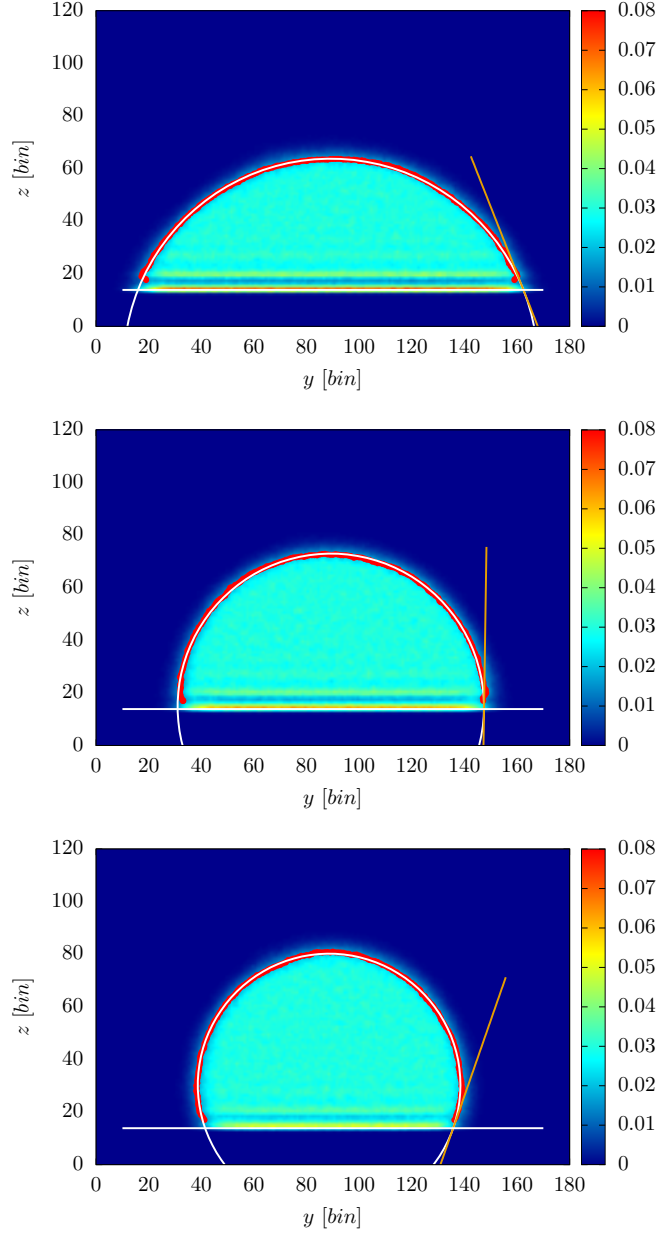
Figure ESI1: To compute the Young contact angle of a surface we deposit a cylindrical water droplet on it, thermalize the system and subsequently compute the average (discretized) density field. From the density field we can identify the Gibbs dividing surface, i.e. the density isosurface with a value halfway between bulk liquid water and vapor. We then fit this surface with a circumference and compute the corresponding tangent formed with the graphite slab. In the panels of this figure we show the density field, Gibbs dividing surface and tangent of three droplets with a Young contact angle of 70° (top), 90° (central) and 110° (bottom).
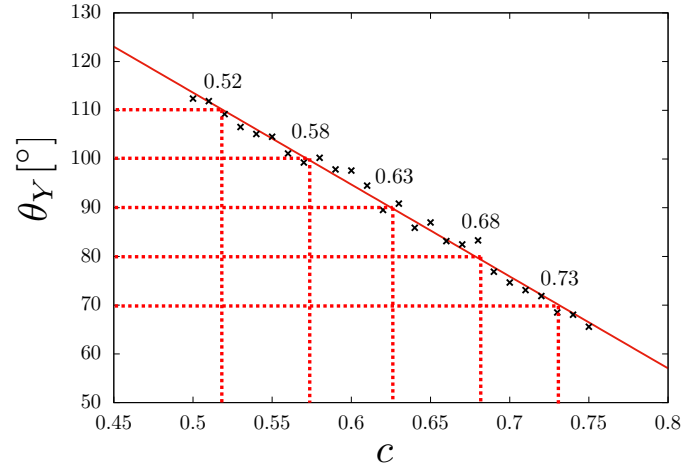
Figure ESI2: Young contact angle θ_Y *vs* the scaling parameter c. The calculations show that there is a linear relation between θ_Y and c over a wide range enclosing the one spanned in our simulations, $[70°, 110°]$. From the linear fitting of simulation data one can determine the value of c necessary to model a solid with a prescribed value of θ_Y.
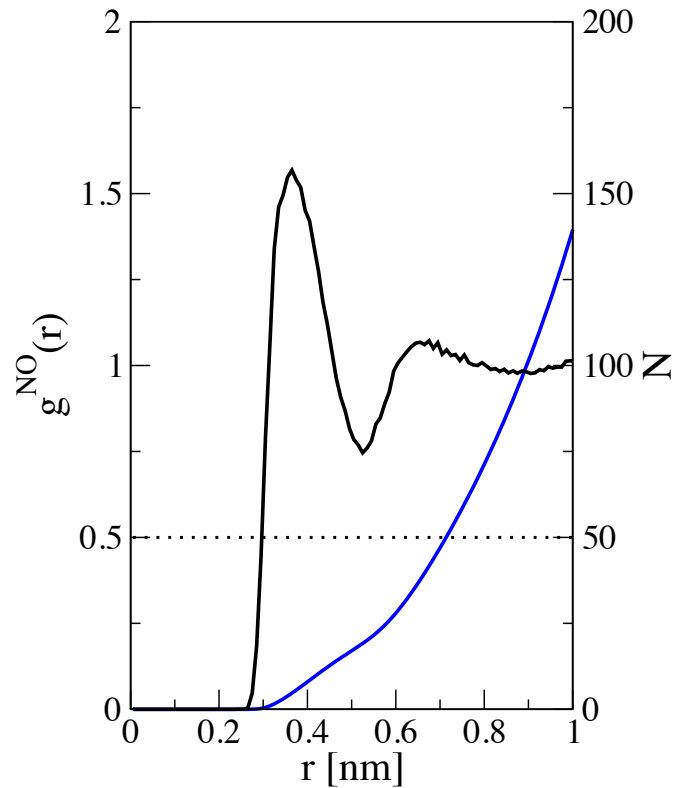
Figure ESI3: Nitrogen-oxygen pair correlation function of an N_2 molecule in bulk water (black) and the corresponding integral, i.e. the number of water molecules within a distance r from N_2 (blue). The dotted line corresponds to 50 nearest neighbor water molecules and is shown to help the reader to appreciate the radius of the shell enclosing the number of water molecules per N_2 at the maximum local oversaturation for a $\zeta = 0$ bulk.
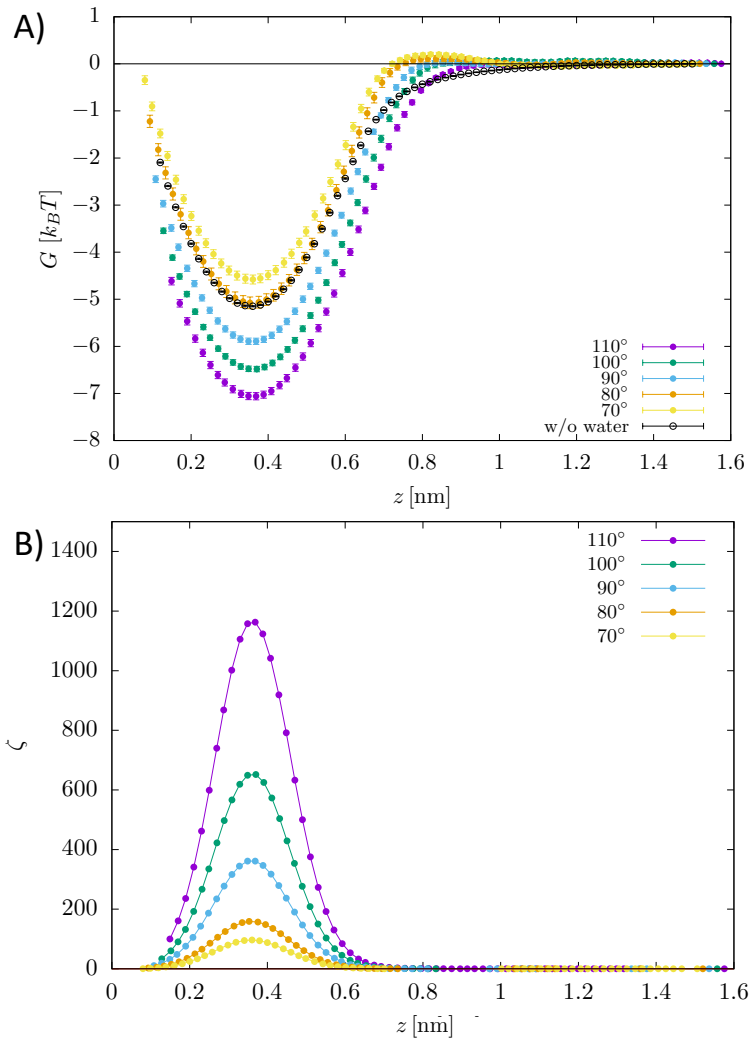
Figure ESI4: A) Free energy $G(z)$ as a function of the distance of the center of mass of the O_2 molecule from the graphite-like surface. In the figure, $G(z)$ is reported for several values of hydrophilicity/hydrophobicity of the surface together with the case without water, i.e. when the sample consists only of the graphite-like slab and O_2. One notices that the profiles are very similar to the N_2 case reported in the main text. B) Supersaturation of O_2 as a function of the distance from the surface.

References

(1) Giacomello, A.; Meloni, S.; Chinappi, M.; Casciola, C. M. Cassie–Baxter and Wenzel states on a nanostructured surface: phase diagram, metastabilities, and transition mechanism by atomistic free energy calculations. *Langmuir* **2012**, *28*, 10764–10772.

(2) Amabili, M.; Giacomello, A.; Meloni, S.; Casciola, C. M. Intrusion and extrusion of a liquid on nanostructured surfaces. *Journal of Physics: Condensed Matter* **2016**, *29*, 014003.

(3) Amabili, M.; Giacomello, A.; Meloni, S.; Casciola, C. M. Unraveling the Salvinia Paradox: Design Principles for Submerged Superhydrophobicity. *Advanced Materials Interfaces* **2015**, *2*, 1500248.

(4) Amabili, M.; Meloni, S.; Giacomello, A.; Casciola, C. M. Activated Wetting of Nanostructured Surfaces: Reaction Coordinates, Finite Size Effects, and Simulation Pitfalls. *Journal of Physical Chemistry B* **2017**, *122*, 200–212.

(5) Amabili, M.; Giacomello, A.; Meloni, S.; Casciola, C. M. Collapse of superhydrophobicity on nanopillared surfaces. *Physical Review Fluids* **2017**, *2*, 034202.

(6) Lisi, E.; Amabili, M.; Meloni, S.; Giacomello, A.; Casciola, C. M. Self-Recovery Superhydrophobic Surfaces: Modular Design. *ACS Nano* **2018**, *12*, 359–367.

(7) Janke, W. Statistical analysis of simulations: Data correlations and error estimation. *Quantum Simulations of Complex Many-Body Systems: From Theory to Algorithms* **2002**, *10*, 423–445.

(8) Tan, B. H.; An, H.; Ohl, C.-D. Surface nanobubbles are stabilized by hydrophobic attraction. *Physical review letters* **2018**, *120*, 164502.

(9) Lohse, D.; Zhang, X. Pinning and gas oversaturation imply stable single surface nanobubbles. *Physical Review E* **2015**, *91*, 031003.

(10) Popov, Y. O. . Evaporative deposition patterns: Spatial dimensions of the deposit. *Phys. Rev. E* **2005**, *71*, 036313.

(11) Wilhelm, E.; Battino, R. Estimation of Lennard-Jones (6, 12) Pair Potential Parameters from Gas Solubility Data. *The Journal of Chemical Physics* **1971**, *55*, 4012–4017.

(12) Reiss, H. Scaled particle methods in the statistical thermodynamics of fluids. *Advances in Chemical Physics* **1965**, 1–84.